Research Article | Vol. 25, No. 6 | 20 Mar 2017 | OPTICS EXPRESS 5962

Optics EXPRESS

Flexoelectric in-plane switching (IPS) mode with ultra-high-transmittance, low-voltage, low-frequency, and a flicker-free image

MINSU KIM,[1,2] HYEONG GYUN HAM,[1] HAN-SOL CHOI,[1] PHILIP J. BOS,[3] DENG-KE YANG,[3] JOONG HEE LEE,[1] AND SEUNG HEE LEE[1,*]

[1]*Applied Materials Institute for BIN Convergence, Department of BIN Convergence Technology and Department of Polymer Nano-Science and Technology, Chonbuk National University, Jeonju, Jeonbuk 561-756, South Korea*

[2]*Current affiliation: Department of Physics and Astronomy, Johns Hopkins University, Baltimore, MD 21218, USA*

[3]*Liquid Crystal Institute, Kent State University, Kent, OH 44242, USA*

[*]*lsh1@chonbuk.ac.kr*

Abstract: The demands for a power-saving mode for displaying static images are ubiquitous not only in portable devices but also in price tags and advertising panels. At a low-frequency driving in liquid crystal displays (LCDs) for low-power consumption, the flexoelectric effect arises even in calamitic liquid crystals and the optical appearance of this physical phenomenon is found to be unusually large, being noticed as an image-flickering. Although the inherent integrated optical transmittance of in-plane switching (IPS) mode is relatively lower than that of fringe-field switching (FFS) mode, the IPS mode shows no static image-flickering but an optical spike (the so-called optical bounce), at the transient moment between signal positive and negative frames. Here, we demonstrate an IPS mode using negative dielectric anisotropy of liquid crystals ($\Delta\varepsilon < 0$) and fine-patterned electrodes (the width w of and the space l between electrodes ≤ 3 μm) with reduced operation voltage (up to 40.7% to a conventional FFS mode with $\Delta\varepsilon < 0$), reduced optical bounce (up to 4.4%. to a conventional FFS mode with $\Delta\varepsilon < 0$) and enhanced transmittance (up to 32.1% to a conventional IPS mode with $\Delta\varepsilon > 0$). We believe the result will contribute not only to the scientific understanding of the optical appearance of flexoelectric effect but also pave the way for engineering of a superior low-power consumption LCD.

OCIS codes: (160.3710) Liquid crystals; (230.2090) Electro-optical devices; (230.3720) Liquid-crystal devices.

References and links

1. T. Tsuruma, Y. Goto, A. Higashi, M. Watanabe, H. Yamaguchi, T. Tomooka, and H. Kikkawa, "Novel image sticking model in the fringe field switching mode based on the flexoelectric effect," in *EuroDisplay* (2011), pp. 13–16.
2. R. Hatsumi, S. Fukai, Y. Kubota, A. Yamashita, M. Jikumaru, H. Baba, K. Moriya, D. Kubota, K. Kusunoki, Y. Hirakata, J. Koyama, S. Yamazaki, Y. Chubachi, and C. Fujiwara, "FFS-mode OS-LCD for reducing eye strain," J. Soc. Inf. Disp. **21**(10), 442–450 (2013).
3. I. H. Jeong, I. W. Jang, D. H. Kim, J. S. Han, B. V. Kumar, S. H. Lee, S. H. Ahn, S. H. Cho, and C. Yi, "P.101: Investigation on Flexoelectric Effect in the Fringe Field Switching Mode," SID Symp. Dig. Tech. Pap. **44**, 1368–1371 (2013).
4. J.-W. Kim, T.-H. Choi, T.-H. Yoon, E.-J. Choi, and J.-H. Lee, "Elimination of image flicker in fringe-field switching liquid crystal display driven with low frequency electric field," Opt. Express **22**(25), 30586–30591 (2014).
5. H. Chen, F. Peng, M. Hu, and S.-T. Wu, "Flexoelectric effect and human eye perception on the image flickering of a liquid crystal display," Liq. Cryst. **42**(12), 1730–1737 (2015).
6. D.-J. Lee, G.-Y. Shim, J.-C. Choi, J.-S. Park, J.-H. Lee, J.-H. Baek, H. C. Choi, Y. M. Ha, A. Ranjkesh, and H.-R. Kim, "Transient flickering behavior in fringe-field switching liquid crystal mode analyzed by positional asymmetric flexoelectric dynamics," Opt. Express **23**(26), 34055–34070 (2015).
7. S.-W. Oh, J.-H. Park, J.-H. Lee, and T.-H. Yoon, "Elimination of image flicker in a fringe-field switching liquid crystal display by applying a bipolar voltage wave," Opt. Express **23**(18), 24013–24018 (2015).
8. H. S. Choi, J. H. Kim, H. G. Ham, Y. J. Lim, J. M. Lee, H. S. Jin, R. Manda, M. S. Kim, D.-K. Yang, and S. H.

#284772 https://doi.org/10.1364/OE.25.005962
Journal © 2017 Received 17 Jan 2017; revised 28 Feb 2017; accepted 1 Mar 2017; published 6 Mar 2017

Optics EXPRESS

Lee, "P-131: Studies on Flickering in Low Frequency Driven Fringe-Field Switching (FFS) Liquid Crystal Display," SID Symp. Dig. Tech. Pap. **47**, 1610–1613 (2016).
9. A. Buka and N. Eber, *Flexoelectricity in Liquid Crystals: Theory, Experiments and Applications* (World Scientific, 2012).
10. M. S. Kim, P. J. Bos, D.-W. Kim, D.-K. Yang, J. H. Lee, and S. H. Lee, "Flexoelectric effect in an in-plane switching (IPS) liquid crystal cell for low-power consumption display devices," Sci. Rep. **6**, 35254 (2016).
11. R. B. Meyer, "Piezoelectric Effects in Liquid Crystals," Phys. Rev. Lett. **22**(18), 918–921 (1969).
12. W. Helfreich, "The Strength of Piezoelectricity in Liquid Crystals," Z. Naturforsch. A **26**(5), 833–835 (1971).
13. J. Prost and P. S. Pershan, "Flexoelectricity in nematic and smectic-A liquid crystals," J. Appl. Phys. **47**(6), 2298–2312 (1976).
14. M. Oh-e and K. Kondo, "Electro-optical characteristics and switching behavior of the in-plane switching mode," Appl. Phys. Lett. **67**(26), 3895–3897 (1995).
15. M. S. Kim, P. J. Bos, D.-W. Kim, C.-M. Keum, D.-K. Yang, H. G. Ham, K.-U. Jeong, J. H. Lee, and S. H. Lee, "Field-symmetrization to solve luminance deviation between frames in a low-frequency-driven fringe-field switching liquid crystal cell," Opt. Express **24**(26), 29568–29576 (2016).
16. K. S. Ha, C. W. Woo, S. S. Bhattacharyya, H. J. Yun, H. S. Jin, Y.-K. Jang, and S. H. Lee, "Analysis of optical bounce associated with two- step molecular reorientation in the fringe-field switching mode," Liq. Cryst. **39**(1), 39–45 (2012).
17. S. H. Lee, S. L. Lee, and H. Y. Kim, "Electro-optic characteristics and switching principle of a nematic liquid crystal cell controlled by fringe-field switching," Appl. Phys. Lett. **73**(20), 2881–2883 (1998).
18. M. Bremer, M. Klasen-Memmer, D. Pauluth, and K. Tarumi, "Novel liquid-crystal materials with negative dielectric anisotropy for TV application," J. Soc. Inf. Disp. **14**(6), 517 (2006).
19. H. Chen, M. Hu, F. Peng, J. Li, Z. An, and S.-T. Wu, "Ultra-low viscosity liquid crystal materials," Opt. Mater. Express **5**(3), 655 (2015).

1. Introduction

Displaying images in a liquid crystal display (LCD) by an active matrix requires a proper driving scheme, which will consume the electric power described as $P = fCV^2$ where f is a driving frequency, C is a capacitance of a panel, and V is the applied voltage. This formula implies that not only a driving voltage but also a driving frequency is important for reducing the power consumption. In general, the driving frequency of LCDs is usually higher than 60 Hz, which means, ideally, the power consumption would become 60 times less by reducing the driving frequency up to near 1 Hz. Such a low-frequency driving may not be proper to displaying fast videos or animated images, but enough to display static images. In regards to the recent low-frequency driving of fringe-field switching (FFS) mode, the flexoelectric effect has been previously considered as a cause of the image-flickering issue of LCDs [1–8]. The polarization induced by flexoelectric effect can be determined as $P_f = e_s \boldsymbol{n}(\nabla \cdot \boldsymbol{n}) + e_b \boldsymbol{n} \times (\nabla \times \boldsymbol{n})$, where e_s and e_b are splay and bend flexoelectric coefficients, respectively, and $\boldsymbol{n}$ is a unit vector of liquid crystal orientation, so-called a director. The calamitic zero-field averaged molecular shape of a nematic liquid crystal has head-tail symmetry; however, under a low-frequency driving, a liquid crystal director can have sufficient time to respond within a single frame to the polarity of the applied field so that the averaged head-tail symmetry can be broken. In this regime, the free energetic description includes three theoretical terms: quadratic dielectric coupling $f_{dielec} = -\frac{1}{2}\varepsilon_0 \Delta\varepsilon (\boldsymbol{n} \cdot \boldsymbol{E})^2$, elastic free energy density $f_{elas} = \frac{1}{2}\left(K_{11}[\nabla \cdot \boldsymbol{n}]^2 + K_{22}[\boldsymbol{n} \cdot (\nabla \times \boldsymbol{n})]^2 + K_{33}[\boldsymbol{n} \times (\nabla \times \boldsymbol{n})]^2\right)$, and linear flexoelectric coupling $f_{flexo} = -[e_s \boldsymbol{n}(\nabla \cdot \boldsymbol{n}) + e_b \boldsymbol{n} \times (\nabla \times \boldsymbol{n})] \cdot \boldsymbol{E}$, where ε_0, $\Delta\varepsilon$, and $\boldsymbol{E}$ denote dielectric constant, dielectric anisotropy of liquid crystals, and an applied electric field. The splay, twist, and bend elastic constants of liquid crystals are denoted by K_{ii} with i = 1, 2, and 3, respectively. To minimize the free energy of such a system, the elastic deformation takes place to compensate the cost of flexoelectric and dielectric effects [9–12].

In an in-plane switching (IPS) mode, the electric potential is periodic in two-dimensional (2D) space with respect to width w of the electrodes and space l between them [10,13,14]; as it is in the FFS mode. At low f and a positive frame (electric field directions are from signal- to common-electrodes) in IPS mode, the flexoelectric polarization becomes *constructive* at

Optics EXPRESS

the region above signal-electrodes but *destructive* at the region above common-electrodes. As a result, the tilt deformation becomes suppressed on the area above common-electrodes so that the plateau of the local transmittance curve, which is located between electrodes without flexoelectric effect, is shifted on to the common-electrodes. The system governed by not only the quadratic dielectric effect but also the linear flexoelectric effect thus attributes doubled periodicity of spatial oscillation of refractive index than only governed by the dielectric effect (In IPS mode, the periodicities are $(w + l)$ and 2 $(w + l)$ without and with flexoelectric effect, respectively, and in FFS mode, those are $(w + l) / 2$ and $(w + l)$, respectively). Unlike in FFS mode, there is no static image-flickering in IPS mode because the brightness of each frame is almost similar owing to the symmetry of electric potential between frames in opposite signs [10,15]. Although this is a huge advantage from a perspective of image-quality, the inherent integrated optical transmittance of IPS mode in general is less than that of FFS mode. This is because, in the conventional IPS mode, the director's twist deformation mainly takes place in the space between electrodes but not in the area above electrodes, which badly affects the integrated transmittance. Because transmittance of FFS mode is higher than that of the IPS mode, the FFS mode is the currently preferred mode for portable devices. The only way the IPS mode can achieve high transmittance and competed with the FFS mode is to reduce both w and l. In this way, the electric fields with fine-patterned electrodes are intensified at the bottom near the electrodes; thus, strengthened torques can be delivered from the space between electrodes to the area above electrodes. Consequently, this twist above the electrodes can also contribute to the local transmittance, and influences the integrated transmittance to be as high as that in the FFS mode.

Here, we propose an IPS mode with high-transmittance (competitive to that of FFS mode) that does not have the image-flickering issue associated with flexoelectric effect. Our proposed device uses negative dielectric anisotropy liquid crystals and intensified electric fields from fine-patterned electrodes (w and $l \leq 3$ μm). In this system, we expect the intensified field at the bottom would give rise to more twist deformation, at the same time, less tilt deformation of directors over the almost entire cell area. Moreover, this effect would be enhanced by adoption of the negative dielectric anisotropy of liquid crystals. Therefore, high-transmittance can be achieved not having static image-flickering. However, owing to the above-mentioned spatially non-uniform electric potential, a coupling between the flexoelectric polarization and an applied electric field is in *constructive* and *destructive* relation according to each frame [10,15]. Thus, an optical spike (the so-called optical bounce [16]), could occur at a frame-transient moment and it could damage the image-quality as a dynamic image-flickering. Reducing this optical bounce would synergistically give rise to realize power-saving displays with record-breaking high-transmittance with no image-flickering in IPS mode with respect to the flexoelectric effect by low-frequency driving.

The next section 2 consists of three subsections; subsection 2.1 will first discuss relevant details of the IPS mode and demonstrate how it can be used to eliminate the flexoelectric induced flicker found in FFS devices. Subsection 2.2 will further show how the transient optical bounce can be removed, and subsection 2.3 will summarize the results of this paper and demonstrate the significant advantages of the device design shown here.

2. Results and discussion

2.1 Eliminating the flexoelectric flicker with an IPS mode, while preserving high optical transmission found in the FFS mode

An IPS cell was prepared as schematically illustrated in Fig. 1(a). Interdigitated signal- and common-electrodes with w (l) = 5 (5) μm were prepared by photo-lithography of transparent indium-tin-oxide layer on a glass substrate. A rubbing process was done at the rubbing angle $\alpha = 7°$ to the long-direction of electrodes after a homogeneous alignment layer of polyimide was spin-coated on both substrates. A nematic liquid crystal (MLC-6252, Merck) was

Optics EXPRESS

injected into a unit cell with the cell gap d, which is maintained by ball spacers with the diameter of 4 μm. Using a high-speed camera (Phantom v211, Vision Research), polarizing optical microscopy (POM) images were systematically acquired (under 200 frames per second (fps) with the exposure time < 5 ms) while applied voltages were alternating in positive (+) and negative (-) frames with a driving frequency f = 60, 30, and 10 Hz. The dynamic response of the prepared cell, which was sandwiched between crossed polarizers, was measured by an automated system for the voltage-application and the photo-detection, that is, combination of a 1° narrow-angle luminance probe (J6523, Tektronix) and a tungsten-halogen light source (Radiometric fiber optic illuminator 77501, Oriel; filtered by monochromatic wave λ = 554 nm). On the other hand, a numerical simulation was done by a commercialized solver using a multi-dimensional finite element method (FEM) (TechWiz LCD, Sanayi system). The electric potential distribution was evaluated based on Laplace's equation, and optical images were calculated based on the [2 × 2] extended Jones matrix method. The dielectric anisotropy $\Delta\varepsilon$ (rotational viscosity γ_1) of liquid crystal were set by 15.3 (89 mPas) and the flexoelectric coefficients were set by e_s (e_b) = 0 (0) and 15 (−5) pC/m without and with flexoelectric effect, respectively; other properties of liquid crystals were identical to those used in the experiment.

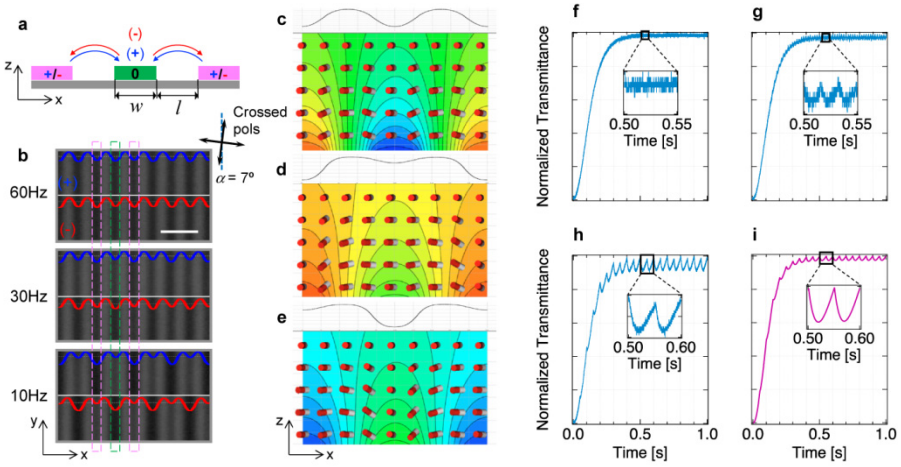

Fig. 1. Flexoelectric effect in an IPS liquid crystal cell. (a) Schematics of cell structure and electric fields in (+) and (-) signal frames. (b) POM images driven at f = 60, 30, and 10 Hz at 3.5 V (50% of maximum transmittance). The pink- and green-dotted rectangles indicate the location of signal- and common-electrodes; the blue- and red-curves indicate local transmittance. Scale bar is 20 μm. (c-e) Simulated director fields where (c) e_s (e_b) = 0 (0), and 15 (−5) in (d) (+) and (e) (-) frames. (f-h) Measured time-dependent transmittance at f = (f) 60, (g) 30, and (h) 10 Hz at 3.5 V. (i) A FEM result of time-dependent transmittance at f = 10 Hz.

The electric field direction in (+) and (-) frames are indicated by the blue- and red-arrows in Fig. 1(a) where the voltage is swung at a signal-electrode. At f = 10 Hz in Fig. 1(b), the flexoelectric coupling became apparently noticed such that the local transmittance (the blue- and red-curves in (+) and (-) frames) is spatially fluctuated according to the location of signal- and common-electrodes indicated by the pink- and green-dotted rectangles, respectively. The sinusoidal behavior of local brightness at f = 60 Hz becomes broken at f = 10 Hz and the repeated displacement becomes twice owing to the linear flexoelectric coupling. The detailed liquid crystal director fields with respect to the electric potential distribution demonstrate the behavior of local transmittance without flexoelectric effect in Fig. 1(c) and with flexoelectric effect at (+) and (-) frames in Figs. 1(d) and 1(e), respectively. Upon the directions of the flexoelectric polarization and electric fields, the splay and bend deformations become either constructive or destructive. Thus, at the destructive

Optics EXPRESS

region (where the opposite directions between the flexoelectric polarization and electric fields), the director tilt is suppressed so that the twist deformation compensates the energetic cost of dielectric effect [10].

As f is reduced from 60 to 30 and 10 Hz, the fluctuation of brightness becomes severe as indicated in the measured time-dependent transmittance in Figs. 1(f)-1(h), and it is clearly related to the longer interval between the frame-transition at the lower-frequency. Moreover, the behavior of the curve at f = 10 Hz is in a good agreement with the numerical calculation as shown in Fig. 1(i) although the magnitude of the fluctuation looks higher in the experimental result seemingly owing to the signal noise.

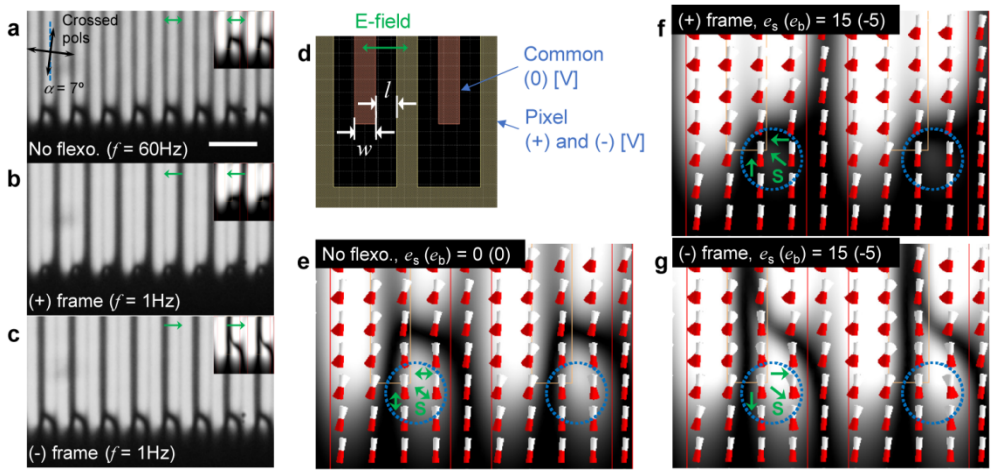

Fig. 2. Investigation between POM images and 3D FEM simulation. (a-c) POM images of an IPS cell (a) without and (b, c) with flexoelectric effect according to interdigitated electrodes including the edge region driven at f = 1 Hz at 3.5 V. Scale bar is 30 μm. Insets show corresponding images calculated. (d) The electrode structure for the simulation. (e-g) Detailed director fields according to the optical appearance in 3D FEM results. The green-arrows indicate electric fields in the blue-circles.

Remarkably, the experimental observation with POM images [Figs. 2(a)-2(c)] is in an excellent agreement with the 3D FEM simulation results [insets in Figs. 2(a)-2(c)], which are done by designed interdigitated electrodes including the edge region in Fig. 2(d) where the green-arrows indicate the direction of electric fields. The agreement between numerical and experimental results consists of three-cases: without flexoelectric effect (f = 60 Hz) in Fig. 2(a), with flexoelectric effect (f = 1 Hz) in (+) and (-) frames in Figs. 2(b) and 2(c), respectively. The detailed liquid crystal director fields are evaluated in Figs. 2(e)-2(g). In Fig. 2(e), the main reason of the different optical appearance, especially the region near the edge (indicated by S in blue-circles), seems caused by the electric field at the vertex of the electrodes. This bright state in S is isolated as an island, and the reason seems that the twist of directors is in the opposite sense to the other area, thereby showing the dark state surrounding the island. Next, as flexoelectric coefficients become non-zero as e_s (e_b) = 15 (–5) pC/m, in (+) frame, this island is reduced in size [Fig. 2(f)] whereas it is expanded in (-) frame [Fig. 2(g)]. This size change is caused by the same mechanism that the local transmittance is spatially shifted due to the constructive and destructive couplings as shown in Figs. 1(b), 2 (b) and 2(c).

Based on the consistency between the experiment and the calculation, we numerically evaluate static and dynamic electro-optic responses of four-general cases: FFS (w (l) = 3 (4.5) μm) and IPS (w (l) = 5 (5) μm) with positive and negative liquid crystals (pLC and nLC) as shown in Fig. 3. From the results, we can summarize four-facts: 1) The maximum transmittance T_{max} of the FFS modes is higher than that of the IPS modes, and for the FFS

Optics EXPRESS

modes, the T_{max} is higher when using nLC than using pLC, but for the IPS modes, it is almost similar for using both nLC and pLC in these particular cases. 2) The operation voltage is lower using pLC in both FFS and IPS modes. 3) There is no deviation of T_{max} between (+) and (-) frames in IPS mode unlike in FFS mode, which means, FFS mode exhibits a static image-flicker [15]. 4) At the frame-transient moment in dynamic responses, there is an optical bounce [16], which can possibly cause a dynamic image-flicker, and it is relatively higher in FFS mode than in IPS mode. As a strategy to realize transmittance as high as that of the FFS mode with nLC, V_{op} as low as that of the IPS mode with pLC, and low optical bounce with no brightness difference between frames, we propose to utilize fine-patterned electrodes and nLC in an IPS mode.

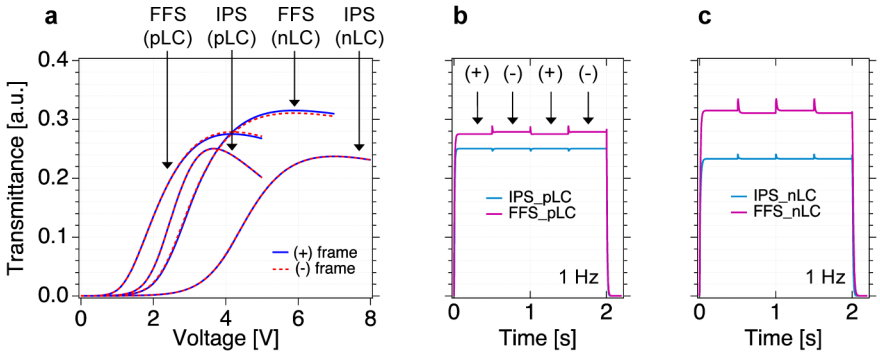

Fig. 3. Static and dynamic electro-optic responses of IPS (w (l) = 5 (5) μm) and FFS (w (l) = 3 (4.5) μm) modes with positive (pLC) and negative (nLC) dielectric anisotropy of a liquid crystal medium governed by combination of linear and quadratic couplings. (a) Voltage-dependent transmittance and (b) time-dependent transmittance of four-cases: (b) FFS-pLC and IPS-pLC; (c) FFS-nLC and IPS-nLC.

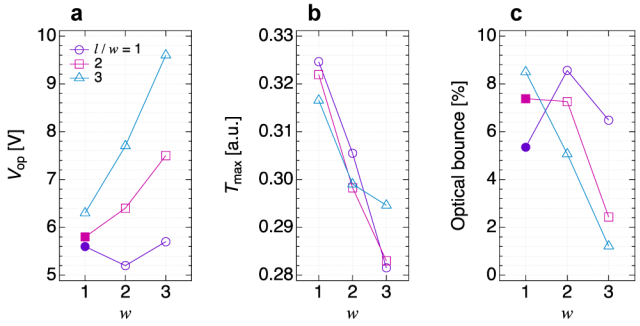

Fig. 4. Electro-optic characteristics of IPS mode with nLC ($\Delta\varepsilon$ = - 3.2, γ_1 = 94 mPas, and e_s (e_b) = 5 (10) pC/m) upon fine-patterned electrodes. (a) V_{op}, (b) T_{max} and (c) corresponding optical bounce with respect to l / w (= 1, 2 and 3) and w (= 1, 2 and 3 μm). The filled-markers indicate the points in a regime where $1 \geq (w + l) / d$.

The summary of calculated V_{op}, T_{max} and optical bounce is shown in Fig. 4 with various structural conditions: w = 1, 2, 3 μm and l / w = 1, 2, 3 using nLC ($\Delta\varepsilon$ = - 3.2, γ_1 = 94 mPas, and e_s (e_b) = 5 (10) pC/m). The calculated optical bounce is defined as the ratio of the momentarily maximum transmittance (peak transmittance) to the saturated transmittance in the most of the frame time. At first, in Fig. 4(a), V_{op} is reduced as w (l) gets reduced (except for the points with filled-markers) and it seems following the conventional tendency of IPS mode, that is, as l gets longer, electric field strength becomes weaker so that V_{op} increases. Second, in Figs. 4(b) and 4(c), T_{max} and optical bounce tend to become higher as w (l) gets reduced (except for the points with filled-markers). One can analyze and discuss on this result as following. According to reports on the theoretical analysis of the conventional IPS mode

Optics EXPRESS

under an applied voltage [14,17], the twist deformation of directors mainly occurs in the space between electrodes. However, with the fine-patterned electrodes, the strong electric fields are intensified near electrodes at the bottom and the strong torques can be translated from the space between electrodes to the area above electrodes. Thus, it can contribute to the occurrence of local transmittance above the electrodes and give rise to the high-transmittance as competitive to that in the FFS mode. Third, it seems the points with the filled-markers are in different regimes of the electric potential distribution where $1 \geq (w + l) / d$ unlike the other points with the empty-markers. (These points with filled-markers are at w (l) = 1 (1) and 1 (2) for V_{op} in Fig. 4(a) and for optical bounce in Fig. 4(c).)

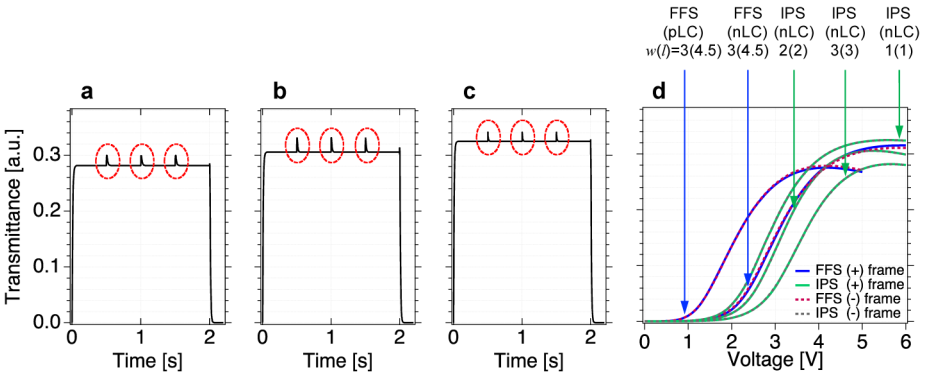

Fig. 5. Time-dependent transmittance of three-cases picked from Fig. 4 using nLC ($\Delta\varepsilon$ = - 3.2, γ_1 = 94 mPas, and e_s (e_b) = 5 (10) pC/m) at an applied voltage for T_{max} with the structural condition (a) w (l) = 3 (3), (b) 2 (2), and (c) 1 (1) μm. Red-dotted-circles indicate the optical bounce [16] at the transient moment between frames at f = 1 Hz. (d) Voltage-dependent transmittance for comparison between the conventional FFS modes from Fig. 3 and the proposed IPS modes.

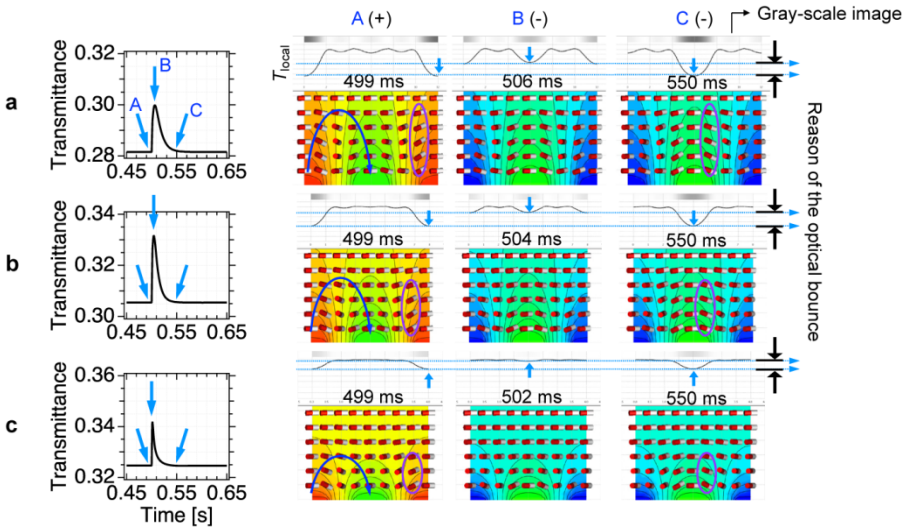

Fig. 6. Investigation of frame-transient moments at (a) w (l) = 3 (3), (b) w (l) = 2 (2), and (c) w (l) = 1 (1). The thinner gray-lines and the thicker blue-lines indicate equipotential area and a representative electric field, respectively. The purple-circles indicate the *constructive* area.

Among those nine-cases in Fig. 4, we pick three-cases in variation of w (l) = (a) 3 (3), (b) 2 (2), and (c) 1 (1) μm and their time-dependent transmittance are shown in Fig. 5. With such fine-patterned electrode structure, the integrated transmittance is achieved with no brightness

Optics EXPRESS

difference between frames, i.e, no static image-flickering, and their integrated transmittances are competitive to that of FFS modes as the voltage-dependent transmittance shown in Fig. 5(d), which consists of the results of both the conventional FFS modes from Fig. 3 ((FFS-nLC and FFS-pLC with w (l) = 3 (4.5) μm) and the proposed IPS modes (IPS-nLC with w (l) = 3 (3), = 2 (2), and = 1 (1) μm). Nevertheless, the optical bounce in these cases become severe unlike the result in Fig. 3, and thus the dynamic image-flickering would occur.

2.2 Method to eliminate the transient optical bounce

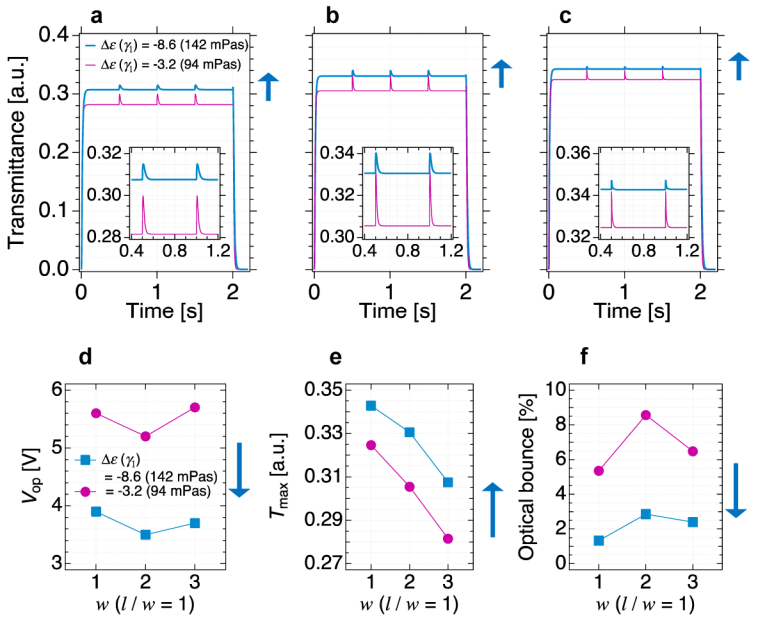

Fig. 7. Enhancement of electro-optic characteristics by increasing dielectric anisotropy and rotational viscosity from $\Delta\varepsilon$ (γ_1) = - 3.2 (94 mPas) to - 8.6 (142 mPas). (a-c) Time-dependent transmittance at an applied voltage for T_{max} with the structural condition w (l) = (a) 3 (3) μm, (b) 2 (2) μm, and (c) 1 (1) μm. (d) Reduced V_{op}, (e) enhanced T_{max}, and (f) reduced optical bounce (dynamic image-flicker).

To eliminate the transient optical bounce, we investigate detailed director field configuration during the frame-transition for w (l) = 3 (3), 2 (2), and 1 (1) μm as shown in Figs. 6(a), 6(b), and 6(c), respectively. By zooming up the time-dependent transmittance curves at f = 1 Hz in Fig. 5, three-moments are labeled by A (the last-scene of (+) frame at 499 ms), B (the scene of the highest bounced brightness in (-) frame at 506, 504 and 502 ms for w (l) = 3 (3), 2 (2) and 1 (1) μm, respectively) and C (the scene of the saturated transmittance in (-) frame at 550 ms). Each scene contains a gray-scale image with respect to the local transmittance T_{local}, and the reason of high-transmittance in IPS mode can be well-unveiled by the results in Fig. 6. From the potential distribution indicated by both the equipotential lines and colors (the thinner gray-solid-lines) and the representative electric fields (the thicker blue-solid-lines), one can recognize the director deformation tends to become intensified at the bottom area as the ratio (w + l) / d becomes low, and such influenced area that the deformation occurs becomes located almost below d / 2 where (w + l) / d becomes less than 1 as indicated by purple-circles in Fig. 6. Thus, the tilt deformation becomes effectively suppressed as vertical components are reduced, and more twist deformation contributes to the transmittance. Furthermore, the reason of the optical bounce is also obviously shown by the director fields at the scenes of A, B and C during the dynamic frame-transition. Upon the frame-transition, the constructive and destructive regions as indicated by the black-dotted-circles are switched by the spatially opposite potential distribution. Here, we note that the constructive and

Optics EXPRESS

destructive couplings are in terms of the direction of electric fields and both splay and bend flexoelectric polarizations. In the dynamic time-evolution, the preceding splay and bend flexoelectric polarizations in the black-dotted-circles at A are released prior to the following flexoelectric polarizations in the black-dotted-circles at C in Fig. 6. At B in between these couplings, the flexoelectric polarizations are suppressed, and thus the twist deformation becomes dominant at the entire region. This integrated transmittance difference gives rise to the optical bounce.

As above-mentioned that the main reason of the optical bounce is the integrated transmittance difference at the moment, i.e, the momentary suppression of the tilt deformation during the switching of the constructive region, we hypothesize continuous suppression of the tilt deformation at the whole frame could give rise to the reduction of the optical bounce; in the meantime, the transmittance increases. To suppress the tilt deformation, we change $\Delta\varepsilon$ and γ_1 of liquid crystals from $\Delta\varepsilon$ (γ_1) = - 3.2 (94 mPas) to - 8.6 (142 mPas), which follows the linear correlation between $\Delta\varepsilon$ and γ_1 [18,19] as shown in Fig. 7. Remarkably, the results show significant enhancement on the electro-optic characteristics: the reduced V_{op}, the increased T_{max}, and the reduced optical bounce in Figs. 7(d), 7(e), and 7(f), respectively.

2.3 Detailed comparison of previous designs with the design proposed in this work

Table 1. Enhanced electro-optic properties.

	Reference				Proposed				Degree of enhancement		
Case	mode	w (l) [μm]	$\Delta\varepsilon$ (γ_1 [Pas])	τ_{rising}[a] ($\tau_{falling}$) [ms]	mode	w (l) [μm]	$\Delta\varepsilon$ (γ_1 [Pas])	τ_{rising} ($\tau_{falling}$) [ms]	V_{op} [%]	T_{max} [%]	Optical bounce [%.]
1	IPS-nLC	3 (3)	- 3.2 (0.094)	18.6 (18.9)	IPS-nLC	3 (3)	- 8.6 (0.142)	25.6 (28.9)	- 35.1	9.2	- 4.1
2		2 (2)	- 3.2 (0.094)	14.0 (19.0)		2 (2)	- 8.6 (0.142)	21.7 (29.2)	- 32.7	8.2	- 5.7
3		1 (1)	- 3.2 (0.094)	15.7 (19.1)		1 (1)	- 8.6 (0.142)	20.8 (29.4)	- 30.4	5.6	- 4.0
4	FFS-nLC	3 (4.5)	- 3.2 (0.094)	18.7 (29.1)	IPS-nLC	2 (2)	- 8.6 (0.142)	21.7 (29.2)	- 40.7	4.9	- 4.4
5	IPS-pLC	5 (5)	15.3 (0.089)	13.5 (15.9)	IPS-nLC	2 (2)	- 8.6 (0.142)	21.7 (29.2)	- 5.4	32.1	1.3

[a]Rising and falling times between 10% and 90% of saturated transmittance at an applied voltage for T_{max}.

Finally, the quantity of the enhanced properties is summarized in Table 1, including the results in which comparing FFS-nLC (w (l) = 3 (4.5) μm) with IPS-nLC (w (l) = 2 (2) μm) and comparing IPS-pLC (w (l) = 5 (5) μm) with IPS-nLC (w (l) = 2 (2) μm). For the cases 1, 2 and 3 in Table 1, V_{op} and optical bounce are reduced up to 35.1% and 4.0%, respectively, and T_{max} increases up to 9.2%, as $\Delta\varepsilon$ is changed from - 3.2 (reference: IPS-nLC) to - 8.6 (proposed: IPS-nLC). For the case 4, V_{op} and optical bounce are reduced up to 40.7% and 4.4%, respectively, and T_{max} increases up to 4.9%, as $\Delta\varepsilon$ is changed from - 3.2 (reference: FFS-nLC, w (l) = 3 (4.5) μm) to - 8.6 (proposed: IPS-nLC, w (l) = 2 (2) μm). For the case 5, although optical bounce increases by 1.3%, V_{op} is reduced by 5.4% and T_{max} increases by 32.1%, as $\Delta\varepsilon$ is changed from 15.3 (reference: IPS-pLC, w (l) = 5 (5) μm) to - 8.6 (proposed: IPS-nLC, w (l) = 2 (2) μm). At last, the rising time τ_{rising} and falling time $\tau_{falling}$ become

Optics EXPRESS

increased as $\Delta\varepsilon$ and γ_1 increase; the average degree of increased rising and falling time is approximately 6.2 and 8.8 ms, respectively. The less increasing in rising time is because the higher γ_1 is compensated by both higher $\Delta\varepsilon$ and the strengthened electric field E in rising time whereas the higher γ_1 is compensated by only higher $\Delta\varepsilon$ in falling time as it is determined by $\tau_{rising} = \frac{\gamma_1}{\varepsilon_0 |\Delta\varepsilon| (E^2 - E_c^{\,2})}$ and $\tau_{falling} = \frac{\gamma_1}{\varepsilon_0 |\Delta\varepsilon| E_c^{\,2}}$ [14].

3. Conclusion

We have proposed a power-saving in-plane switching (IPS) mode governed by flexoelectric effect as well as dielectric effect at low-frequency driving, which shows remarkable electro-optic performances: no brightness difference at frame-transition (no static image-flicker) low operation voltage, ultra-high transmittance, and low optical bounce (low dynamic image-flicker). The results show a practical way to realize low power consumption liquid crystal displays from an engineering perspective. In IPS mode, the electric potential distribution is highly symmetric at positive and negative frames, thereby no static image-flicker. The fine-patterned electrode structure gives rise to the twist deformation at the area not only between electrodes but also above electrodes so that the transmittance is achieved as high as that of fringe-field switching (FFS) mode. Nevertheless, an optical bounce occurs at frame-transient moments, and it is caused by momentary suppression of the localized flexoelectric coupling during the frame-transition. Using high dielectric anisotropy as well as high rotational viscosity of liquid crystals, the director tilt deformation is highly suppressed; therefore, significant reduction on the optical bounce is achieved. The results of this work clearly demonstrate the realization of low power consumption displays, and efficiently give a way to design practical devices through the application of low-frequency and low-voltage driving.

Funding

Basic Research Laboratory Program (2014R1A4A1008140) through the Ministry of Science, ICT & Future Planning; Basic Science Research Program (2016R1D1A1B01007189) through the National Research Foundation of Korea (NRF) funded by Ministry of Education.

Acknowledgments

Prof. D.-K. Yang thanks to the supports from BOE Co.